An Optimal Filter for Geostrophic Mesoscale Currents from Along-Track Satellite Altimetry

BRIAN S. POWELL AND ROBERT R. LEBEN

Colorado Center for Astrodynamics Research, University of Colorado, Boulder, Colorado

(Manuscript received 27 June 2003, in final form 18 March 2004)

ABSTRACT

An optimal difference operator is derived for smoothing along-track sea surface height measurements from satellite altimeters and computing geostrophic surface currents at or below ocean mesoscale wavelengths with second-order approximation accuracy. The difference operator minimizes the white noise of the height measurements to find a compact difference formula for the sea surface height derivative and a residual noise estimate for the surface geostrophic velocity. This compact, optimal operator has fine along-track spatial resolution ideal for studies in areas of shallow water, near landfall, and at high latitudes where the first-baroclinic Rossby radius of deformation becomes small. Accurate extraequatorial geostrophic velocities are determined by varying the filter window to maintain accuracy and resolution, which will benefit global mesoscale studies from the tandem *Jason-1* and TOPEX/Poseidon missions and, particularly, the proposed wide-swath altimetry mission.

1. Introduction

To derive geostrophic currents from satellite altimetry, the measurement noise is reduced with a chosen filter (loess, boxcar, hanning, etc.) followed by a difference operation (least squares slope estimate, finite difference). These techniques have proven useful in oceanographic studies (Morrow et al. 1994; Qiu 1995; Stammer 1997; Strub et al. 1997; Ohlmann et al. 2001). Although these methods are robust and successful, they do not optimally remove the white noise while retaining maximum signal, which is important for studies at oceanic mesoscale wavelengths.

Radar altimeters are affected by internally generated white noise impacting the accuracy of slope estimates in the mesoscale range. This white, instrument noise can dominate errors at these wavelengths because a standard finite-difference operation on the along-track height measurements acts as a high-pass filter. To mitigate the instrument noise, the heights are typically filtered, and further reduction of the noise is possible with longer difference operator lengths. As shown by Strub et al. (1997), differencing over larger point-to-point intervals in the finite-difference operator is equivalent to a running average smoothing of the geostrophic velocities calculated at the midpoints between samples. We have developed an optimal difference operator that in a single operation both optimally reduces the noise and computes the derivative.

For absolute height accuracy, pathlength and environmental corrections (e.g., ionosphere, dry and wet troposphere, sea-state bias, inverted barometer, tide, etc.) are applied to the altimeter range measurements. These corrections are typically of long wavelength, are often unnecessary for slopes computed over shorter length scales, and may increase the noise floor of the slopes without improving the slope accuracy at the mesoscale. A regional height dataset computed solely by subtracting the range measurement from the orbit height may be sufficient for computing accurate slopes over a large range of latitudes.

In this paper, we present a method to calculate a first derivative to second-order approximation accuracy from satellite altimetry heights while minimizing the white noise of the measurements. The technique is useful for the study of shorter wavelength signals such as mesoscale eddies (typically 50–200 km) as well as for coastal and shallow water where corrections and end effects make analysis difficult. In section 3, we present the results of the optimal difference operator, the frequency domain characteristics of the operator, and how they apply to the TOPEX/Poseidon satellite. In section 4, we explain a method of filter size selection suited for mesoscale studies. In section 5, we present evidence for when to apply environmental corrections for mesoscale slope analysis. In section 7, we propose future applications that are well suited to the use of the presented operator. Finally, for those who wish to put the operator to work, the appendixes show a single operator trun-

Corresponding author address: Brian S. Powell, Colorado Center for Astrodynamics Research, University of Colorado, Campus Box 431, Boulder, CO 80309-0431.
E-mail: brian.powell@colorado.edu

cation error example as well as Matlab code to generate the parameters of an optimal operator of any size and window geometry.

2. Derivation of optimal difference operator

Consider the problem of computing a time derivative from regularly sampled height measurements assuming no data outages. Define i to be the current point at which the derivative is being computed, h_i as the height at the current point, and t as time. With this notation, two operators are defined:

$$\Delta_t^+ = \frac{h_{i+1} - h_i}{\Delta t} \quad \text{and} \quad \Delta_t^- = \frac{h_i - h_{i-1}}{\Delta t}, \tag{1}$$

where Δt is the sampling frequency (assumed evenly spaced) of the height data in seconds. From these definitions, a three-point central difference operator with second-order approximation accuracy, $O(\Delta t^2)$, is written as

$$\Delta_{2t}^{-+} = \frac{1}{2}\Delta_t^- + \frac{1}{2}\Delta_t^+, \tag{2}$$

where the scalar factors equally weight each difference term. In many cases (such as data outages, near shelf breaks, etc.), a central difference scheme is not appropriate. Extrapolating (2) into a generic operator gives

$$\Delta_{Nt}^{pq} = \sum_{\substack{n=-p \\ n\neq 0}}^{q} c_n \left(\frac{h_{i+1} - h_i}{n\Delta t} \right), \tag{3}$$

where p and q are the number of points before and after the current point, N is defined as the number of points ($N = p + q$), and the c_n are the currently undetermined weighting coefficients constrained by

$$\sum_{\substack{n=-p \\ n\neq 0}}^{q} c_n = 1. \tag{4}$$

The generalized operator (2) allows for a difference scheme that is not centered; rather, it can be in any configuration about the current h_i location.

For simplicity, collect the h_i terms of (3) separately to find

$$\Delta_{Nt}^{pq} = \left(\sum_{\substack{n=-p \\ n\neq 0}}^{q} \frac{-c_n}{n\Delta t} \right) h_i + \sum_{\substack{n=-p \\ n\neq 0}}^{q} \left(\frac{c_n}{n\Delta t} h_{i+n} \right). \tag{5}$$

Derivation of conventional finite-difference techniques (e.g., Peyret and Taylor 1983) minimizes the truncation error by solving a set of Taylor series expansions to compute weighting coefficients for each term (see appendix A). We must apply a different approach to find the coefficients that minimize the instrument error.

Define δh as the uncertainty present in any measurement of h from the combinations of instrument white noise and colored noise due to correlated errors and noise such as sea state, atmosphere, etc. The corrections for colored noise are well understood and readily available; however, we are concerned with eliminating the white noise. Taylor (1982) states that the total uncertainty for adding independent measurement to be

$$\delta = \sqrt{\sum_{n=-p}^{q} \delta h_n^2}, \tag{6}$$

where δ is the uncertainty of the final result. Define T as the total number of points in the operator, including the point of interest ($T = N + 1$). Because (5) contains scalar factors with each height measurement, the uncertainty calculation (6) becomes

$$\delta v = \delta h \left[\left(\sum_{\substack{n=-p \\ n\neq 0}}^{q} \frac{c_n}{n\Delta t} \right)^2 + \sum_{\substack{n=-p \\ n\neq 0}}^{q} \left(\frac{c_n}{n\Delta t} \right)^2 \right]^{1/2}, \tag{7}$$

where we define δv as the noise in the computed slope value.

Now consider that we wish to minimize the value of δv. The uncertainty in the measured altimeter height value (δh) cannot be minimized as it is a function of the instrument and environmental errors. The minimal value for δv can be found by minimizing

$$\left(\sum_{\substack{n=-p \\ n\neq 0}}^{q} \frac{c_n}{n\Delta t} \right)^2 + \sum_{\substack{n=-p \\ n\neq 0}}^{q} \left(\frac{c_n}{n\Delta t} \right)^2 \tag{8}$$

subject to constraint (4).

The most straightforward method of minimizing this term is to use the method of undetermined multipliers by Lagrange. We introduce the Lagrangian multiplier, λ, and define the Lagrange function as

$$L \equiv \left(\sum_{\substack{n=-p \\ n\neq 0}}^{q} \frac{c_n}{n\Delta t} \right)^2 + \sum_{\substack{n=-p \\ n\neq 0}}^{q} \left(\frac{c_n}{n\Delta t} \right)^2 - \lambda \left(1 - \sum_{\substack{n=-p \\ n\neq 0}}^{q} c_n \right). \tag{9}$$

The objective is to find a set of c_n that minimize L. Differentiating (9) with respect to each c_n and setting the result to zero gives

$$\frac{\partial L}{\partial c_n} = \frac{2}{n\Delta t^2} \left(\sum_{\substack{j=-p \\ j\neq 0}}^{q} \frac{c_j}{j} + \frac{c_n}{n} \right) - \lambda = 0; \tag{10}$$

therefore,

$$c_n = \frac{\lambda n^2 \Delta t^2}{4} - \frac{n}{2} \left(\sum_{\substack{j=-p \\ j\neq\{0,n\}}}^{q} \frac{c_j}{j} \right). \tag{11}$$

Next, sum (11) over all n and use the constraint given by (4) to solve for the Lagrangian multiplier, λ. We are then left with a system of N equations of the form (11) and N unknowns (c_n). The resulting coefficients, c_n, are the optimal coefficients because they minimize the noise, δv, in the slope calculation (5).

This optimal difference operator solves for the max-

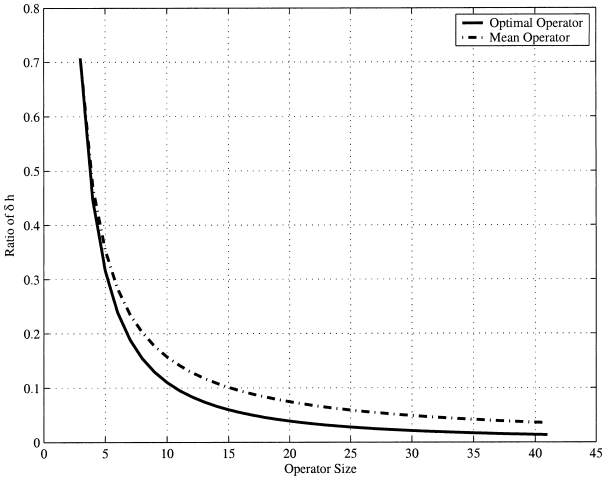

FIG. 1. The decrease in noise vs the number of points used (T) for the optimal and the standard mean operator ($\sqrt{2}/N$) cases.

imum noise reduction possible for a given window size. A conventional central difference operator with equal weighting for each term will cancel all but the end point values, resulting in a noise reduction of

$$\delta v = \delta_h \frac{\sqrt{2}}{N}. \tag{12}$$

3. Results

The properties of the operator have been calculated for all combinations of p and q at varying values of the window width, T. As shown in Fig. 1, the slope noise decreases rapidly through T values of up to 10 points before beginning to level off. As the operator length grows, a trade-off is made between the amount of resolution in the slopes and the slope noise. As shown in the figure, a comparison can be made with the noise reduction from a mean finite-difference operator—with noise defined by (12)—and the optimal difference operator.

The optimal operator (Δ_{Nt}^{pq}) maintains a constant slope noise value for a fixed N and any combination of p and q. This is an important feature of this operator and is useful for applications in satellite altimetry where coastal boundaries, flagged data, etc., create gaps throughout the time series. By taking advantage of the fact that the slope noise remains constant, the filter can vary its window coefficients such that it borders the outage and proceeds on the other side without an increase in slope noise. Keeping a consistent slope error enhances the ability of the operator to compute slopes in coastal regions; however, as will be shown, there can be a resulting phase offset effect caused by varying the window about the point of interest.

As an example, the $T = 5$ case is computed in Table 1. The coefficients are mirrored about the symmetric ($p = q$) case, and allow us to compute the optimal slope using every location before, after, or combinations therein for the currently evaluated location.

TABLE 1. Coefficients for the five-point operator and the resulting noise (factor of $\delta\eta$).

p	q	Coefficients				δv (factor of $\delta\eta$)
4	0	$c_{-4} = 0.8$	$c_{-3} = 0.3$	$c_{-2} = 0.0$	$c_{-1} = -0.1$	0.316
3	1	$c_{-3} = 0.6$	$c_{-2} = 0.2$	$c_{-1} = 0.0$	$c_1 = 0.2$	0.316
2	2	$c_{-2} = 0.4$	$c_{-1} = 0.1$	$c_1 = 0.1$	$c_2 = 0.4$	0.316
1	3	$c_{-1} = 0.2$	$c_1 = 0.0$	$c_2 = 0.2$	$c_3 = 0.6$	0.316
0	4	$c_1 = -0.1$	$c_2 = 0.0$	$c_3 = 0.3$	$c_4 = 0.8$	0.316

The TOPEX/Poseidon (T/P) satellite is a dual-radar altimeter system launched aboard *Ariane 42P* on 10 August 1992 into an orbit with an altitude of 1336 km and an inclination of 66°. The satellite maintains a repeat period of 9.91 days (nominally called a ''10-day cycle'') with an along-track resolution of under 6 km (Fu and Cazenave 2001). The TOPEX altimeter was commissioned by NASA's Jet Propulsion Laboratory (JPL) and the Poseidon altimeter was provided by the French Centre National d'Etudes Spatiales (CNES). These two altimeters share a single antenna, and Poseidon was used to collect 10% of the data. The examples shown in this discussion will only apply to the TOPEX altimeter.

As shown by Fu et al. (1994), the instrument noise, δh, for the TOPEX altimeter is approximately 1.7 cm at an average significant wave height of 2 m. The along-track ground velocity of T/P averages 5.75 km s^{-1} for a sampling frequency of 1 Hz. Table 2 contains results for operator sizes 3 through 21 with the corresponding noise statistics from the TOPEX altimeter.

Frequency diagnostics

Using the techniques shown by Schlax and Chelton (1992), we analyze the optimal difference operator properties in the frequency domain. The frequency domain allows us to understand the transfer function properties of the operator over varying sizes as well as the implications of sliding the filter (varying p and q) about the point of interest. The half-power wavelength for each filter is computed and listed in Table 2. The half-power location specifies the frequency above which all higher frequencies are effectively removed from the signal.

The weights of the optimal difference operator are integrated to find an equivalent smoothing kernel on the heights to inspect the frequency characteristics of the filtering process on the heights. Using these kernels, the passband characteristics for several differently sized operators are shown in Fig. 2.

As the operator size increases, the half-power point decreases in frequency, removing more of the higher frequencies. The average ratio between the window width (in kilometers) of the operator and the half-power wavelength is fairly constant at 0.81. The goal is to

TABLE 2. Properties of various filter window sizes and their application to the TOPEX altimeter. The operator size is the length of the window using T 1-Hz values. The TOPEX altimeter noise corresponds to the total along-track noise of the computed slope ($\delta\eta \approx 17$ mm). The half-power wavelength is based upon the frequency of the filter.

Points (T)	Noise in $\delta\upsilon$ (factor of $\delta\eta$)	Half-power frequency (Hz)	T/P window size (km)	TOPEX altimeter noise (mm s^{-1})	T/P half-power wavelength (km)
3	0.7071	0.3334	11.5062	12.0208	17.2558
4	0.4472	0.2234	17.2593	7.6026	25.7525
5	0.3162	0.1709	23.0124	5.3759	33.6635
6	0.2390	0.392	28.7655	4.0638	41.3297
7	0.1890	0.1178	34.5186	3.2127	48.8379
8	0.1543	0.1022	40.2717	2.6232	56.2926
9	0.1291	0.0903	46.0248	2.1947	63.7110
10	0.1101	0.0810	51.7779	1.8716	71.0259
11	0.0953	0.0734	57.5310	1.6209	78.3801
12	0.0836	0.0671	63.2841	1.4216	85.7392
13	0.0741	0.0619	69.0372	1.2601	92.9418
14	0.0663	0.0574	74.7903	1.1271	100.2282
15	0.0598	0.0535	80.5434	1.1059	107.5346
16	0.0542	0.0501	86.9265	0.9220	114.8323
17	0.0495	0.0471	92.0496	0.8416	122.1465
18	0.0454	0.0445	97.8027	0.7723	129.2831
19	0.0419	0.0421	103.5558	0.7121	136.6532
20	0.0388	0.0400	109.3089	0.6592	143.8275
21	0.0360	0.0381	115.0620	0.6126	151.0000

select an operator size that allows the oceanographic signal to pass through, but removes most of the higher-frequency noise. There are slight sidelobe issues with the shorter length operators; however, as the size increases, these sidelobes are suppressed rather quickly. If very smooth passband characteristics are important, loess filtering is an excellent choice (see Schlax and Chelton 1992). As the size increases, the amount of power allowed through the lower-frequency pass band falls below 1.0, which decreases the power of the lower frequency signals.

The phase angle of the pass bands are similar for centered operators (when $p = q$); however, as the operator is moved about the point of interest, the phase can change dramatically. In Fig. 2, the smoothing kernel for the centered and end point cases ($q = 0$) are shown as solid and dotted lines, respectively. In each case, the transfer function is identical; however, the difference in phase angle for each frequency dramatically increases as the frequency nears the half-power point. At this location, the phase angle can vary by as much as $-140°$ in the sizes presented. If the end point were at the beginning ($p = 0$), the phase shift would be of equal magnitude in the other direction. This can be very important if the energy of interest is at the half-power point. Because of the phase issues, one must decide how to handle data outages and end points. One recommended method is to shorten the operator size as the end point is approached (or from the beginning).

For example, if one is using a 15-point operator ($p = 7$, $q = 7$) and comes upon an end point, rather than keeping a 15-point operator and sliding it off-center until the end point is reached ($p = 14$, $q = 0$), it may be wiser to keep p constant and decrease q. As shown in Table 3, the phase angle of the original half-power location changes 9.61° (for the $T = 15$ case) with each step closer to the end point. The filter size is decreasing at each step while energy in the original half-power is still within the pass band; however, the slope error due to noise increases with decreasing T. If the energy being resolved is of a lower frequency, as shown in Fig. 2, one may not require a changing filter size if the resulting phase shift is small enough.

4. Difference operator size selection

Selecting the proper difference operator size, T, is based upon the requirements of the particular study. An important characteristic of the optimal difference operator is to minimize the noise for a given size. In altimeter applications, this property allows us to choose a length scale that will best resolve the energy of mesoscale eddies.

The first-baroclinic Rossby radius of deformation sets the length scales of the mesoscale wavelengths as a function of geographic location. Chelton et al. (1998) has created a global database for the first-baroclinic Rossby radius of deformation that is used to resolve mesoscale currents. For every h_i location, the operator with a half-power wavelength most closely exceeding twice the first-baroclinic Rossby radius is chosen. This method ensures that we are filtering energy outside of the mesoscale wavelengths of interest on a global basis. In the equatorial region (within 5°), the currents defined by the first-baroclinic Rossby radius become primarily zonal and over 200 km in wavelength. As the presented optimal difference operator was designed to operate at shorter length scales, this region requires other techniques designed to resolve the long-wavelength, zonal nature of the signal.

As shown in Fig. 3, the operator size varies from 3 points to 55 near the equator. The maximum first-baroclinic Rossby radius that we resolve is 200 km (using the 55-point filter with a half-power point of 397 km). The corresponding geostrophic velocity errors due to instrument noise using the operator sized to match the Rossby radius are shown in Fig. 4. As shown, the median geostrophic velocity error for the subtropics (5°–20°) and midlatitudes (20°–60°) is 4.62 cm s^{-1}, which is quite low. As shown in the figure, the error increases with increasing latitude; however, the Rossby radius is decreasing (resulting in a much shorter operator size as in Fig. 3) while the mesoscale signal strength is increasing. If the entire TOPEX coverage area is included (up to 66° without the equatorial region), the median geostrophic velocity error is 5.36 cm s^{-1}.

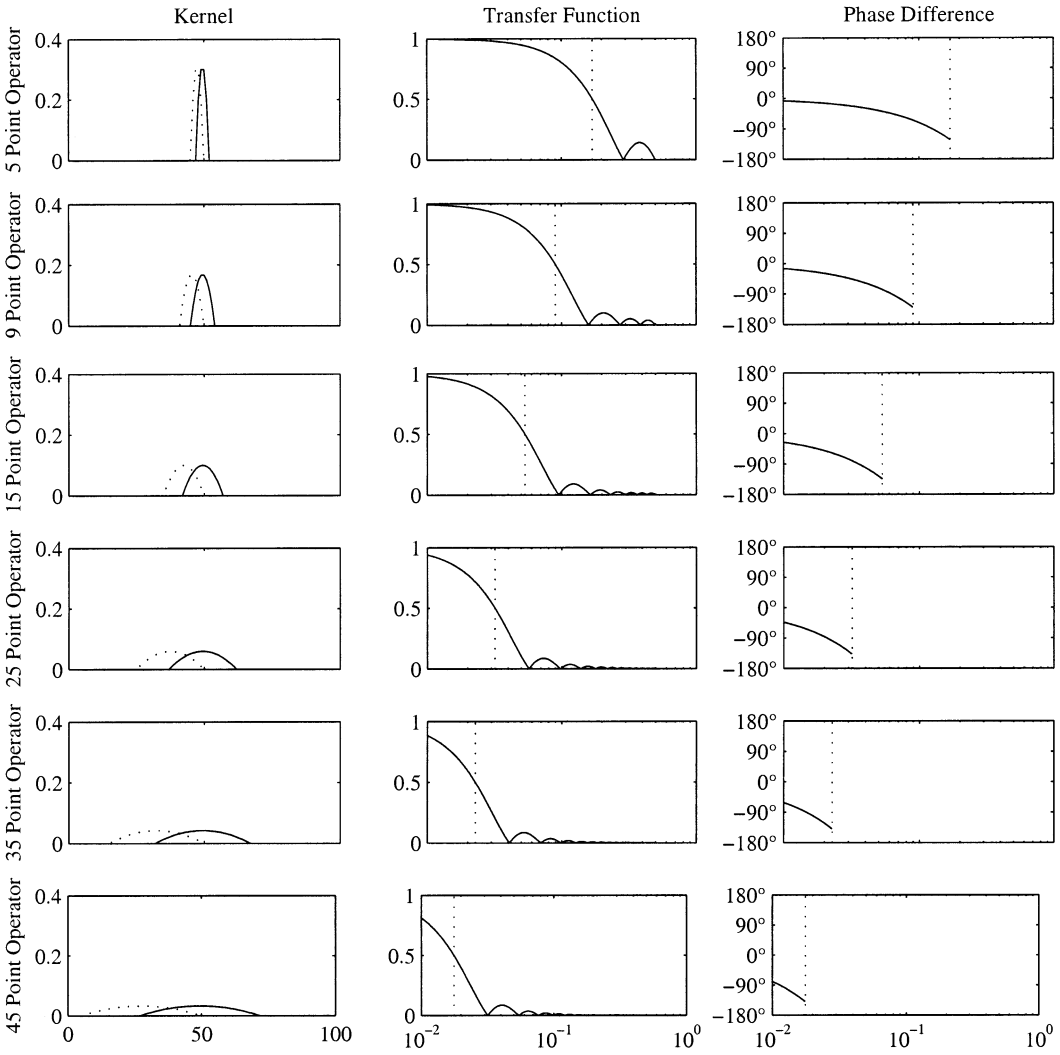

FIG. 2. Equivalent smoothing kernels, transfer functions, and phase angle change between the centered and end cases for several different derivative operators. The smoothing kernel represents the filtering applied in the heights as the derivative is being computed. The estimates are applied to point 50 of a 100-point evenly spaced sample. The dashed line marks the half-power location of the filter.

TABLE 3. The phase angle at the same wavelength as the window size is decreased approaching an end point. Note that with each change the phase angle increases by 9.61°. By carefully varying the window about the point of interest, the phase effects of the changing filter can be mitigated.

Points (T)	p	q	Phase angle (deg)
15	7	7	147.73
14	7	6	157.34
13	7	5	166.95
12	7	4	176.56
11	7	3	−173.83
10	7	2	−164.22
9	7	1	−154.60
8	7	0	−414.99

5. Altimeter corrections

Sea surface height slopes are computed from altimeter data archives that have been corrected to give the most accurate measure of absolute sea level. Depending on the region of interest, this practice may increase the noise in the geostrophic velocity anomalies, requiring excessive smoothing to mitigate. Although a derivative acts as a high-pass filter, high-frequency noise from the corrections can influence the result. Standard altimetric corrections have long signal wavelengths and, as shown by Leeuwenburgh and Stammer (2002), shorter velocity scales are not affected by the orbit or other environmental errors. This consequence of the corrections has been well known in the marine gravity community (Yale et al. 1995) where sea surface slopes are used to calculate anomalies in the gravity field and estimate bottom

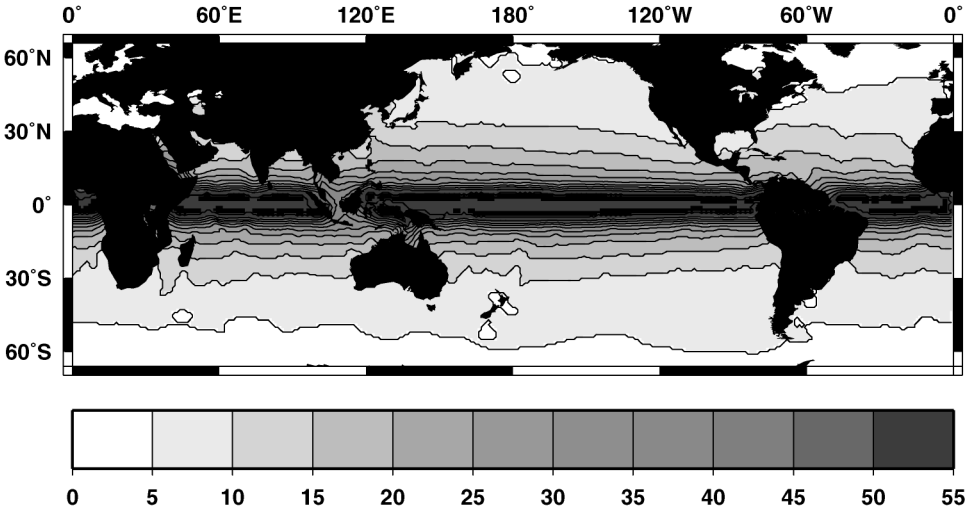

FIG. 3. The number of points (T) used by the filter to resolve the first-baroclinic mode of the Rossby radius of deformation. The equatorial region ($\pm 5°$) is not considered due to the zonal nature of the flow.

topography. By carefully examining the impact of each altimetric correction, Yale (1997) has shown that no corrections are needed in water deeper than 200 m for short-velocity gravity scales.

In the previous section, the first-baroclinic Rossby radius was used to set the operator length for resolving mesoscale energies except in the equatorial region. Applying the optimal operator to each individual correction from TOPEX at these Rossby scales allows us to inspect whether there are any environmental corrections that need to be applied to the data before computing the geostrophic current in the mesoscale. For each correction, the correction slope was computed at every along-track location using the optimal operator over every TOPEX cycle for the 10-yr original T/P mission. The time variability of each location was computed, and the global median variability of each correction is shown in Table 4.

The median variability over the entire 10-yr dataset of the original T/P mission is quite low. Combining the variability of each correction using (6) results in a total geostrophic velocity variability of 2.46 cm s^{-1} for all corrections. Some of the corrections are correlated as shown by Zlotnicki (1994), and combining the individual variabilities as independent measurements is an overestimate of the variability. Therefore, a value of 2.46 cm s^{-1} is a robust overestimate of the variability due to corrections. The variability presented contains both signal and noise of each respective correction, which is important for understanding the energy present. As shown in the previous section, the global median geostrophic velocity variability in the currents due to

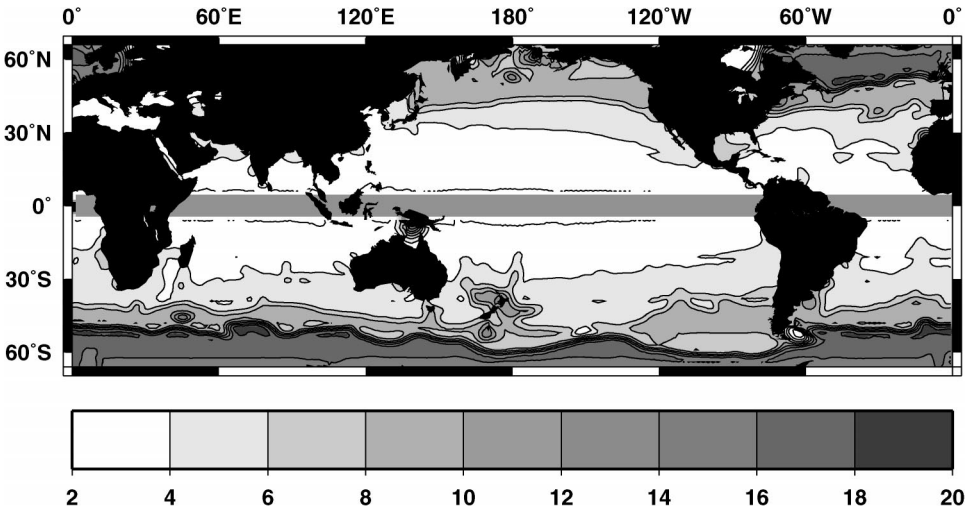

FIG. 4. The slope noise (cm s^{-1}) in the resulting geostrophic current from the matching filter size in Fig. 3. The median error is 5.36 cm s^{-1}. The equatorial region is not considered and is masked out.

TABLE 4. The geostrophic velocity variability of each TOPEX correction over the 10 yr of original mission. Each correction velocity was computed using the method presented, and its variance in time was computed. The table values reflect the global mean (with the 5° equatorial band masked out) of these variances.

Correction	Geostrophic velocity variability (cm s^{-1})
Dry troposphere	0.14
Inverted barometer	0.8
Ionospheric delay	1.31
Ku-band sea-state bias	1.16
Ocean tide	1.18
Pole tide	0.0
Solid earth tide	0.19
Wet troposphere	0.96
Combined error	2.46

instrument noise is 5.36 cm s^{-1}, which is twice as large as the combined correction variability.

The global statistics show that for mesoscale velocities the variability of the signal of the corrections is less than the noise of the instrument, indicating that the corrections do not need to be applied if the signal is strong; unfortunately, on a regional basis, this does not always hold. As mentioned, in the subtropics (less than 20°) the first-baroclinic Rossby radius becomes very long. This length begins to reach the long velocity scales that contain environmental correction energies. As shown in Table 4, the corrections that contain the most variability are ionospheric delay, Ku-band sea-state bias, ocean tide, and wet troposphere. By combining the along-track variabilities of these four corrections using (6), the ratio between the geostrophic velocity variability due to noise and the variability of the corrections can be made.

As shown in Fig. 5, in areas of the subtropics, the ratio of the corrections to the instrument noise is larger than one, requiring that the corrections be applied; otherwise, energy from these corrections would remain in the geostrophic velocity. In regions where the ratio is less than one, the corrections' signal is less than the varibility due to noise and may not be needed for the particular study. These ratios are only applicable if one is resolving mesoscale energies. At length scales shorter than the mesoscale, the need for corrections decreases.

In most regions of the globe, when using the optimal operator, there is no need to apply environmental corrections to the data. Only in the subtropics must one consider the impact that corrections would have upon the resulting mesoscale velocities. When working with the optimal operator in submesoscale and coastal areas, corrections are not required, which is extremely important for operating in these regions due to the large spot size of the microwave radiometers employed to resolve a number of the environmental corrections.

6. Conclusions

This paper presents a novel method of deriving slopes from sea surface heights measured by altimetry. The method maximizes the signal-to-noise ratio by eliminating white noise while calculating slopes over short spatial scales. Slopes can be derived near land and data outages by eliminating the need for corrections and keeping the noise and transfer function consistent over fixed lengths (regardless of orientation but with phase shift consequences). The proper size for

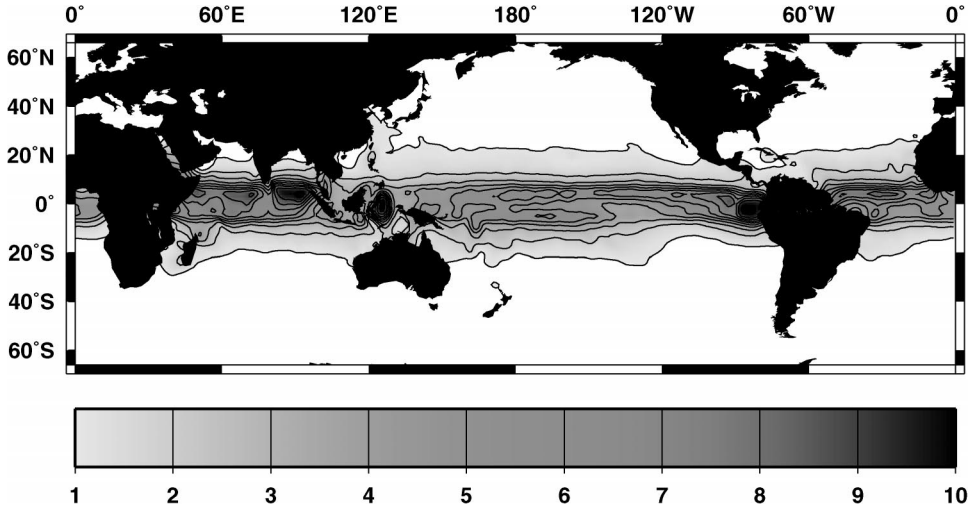

FIG. 5. The ratio of the combined corrections' (wet troposphere, ionosphere, ocean tide, and sea-state bias) velocity variability (noise + signal) vs the theoretical velocity variance due to instrument noise (without signal). Areas greater than one show geographic regions where corrections need to be applied because their signal is larger than the noise signal of the instrument. Notice that for areas of interest outside of the subtropics, corrections typically need not be applied, which is important for studying coastal current.

mesoscale studies at the Rossby radius of deformation can be chosen using the presented frequency domain characteristics.

7. Future work

As shown, a minimal number of 1-Hz heights to generate accurate slopes with minimal error can be achieved. Because the technique developed is independent of corrections and sampling frequency, it could be applied to much higher rate height data, such as 10 Hz from the TOPEX altimeter, 20 Hz from *Jason-1*, and even 40-Hz sea surface height fields from the *Ice, Cloud, and Land Elevation Satellite* (*ICESat*). The error in the 1-Hz field for T/P is given as 1.7 cm (Fu et al. 1994); thus the 10-Hz error would be roughly $1.7\sqrt{10}$. So, to resolve energies at the same wavelength with the 10-Hz data would increase the error by $\sqrt{10}$; however, 10 times as many points would be used in the calculation. Thus, the final velocity error would be identical to the 1-Hz case, but, 10 times as many samples would be used to compute the velocity. This would allow for more detailed submesoscale studies to be performed. Additionally, we have successfully performed preliminary proof of concept studies using *ICESat* 40-Hz sea surface heights to resolve small-scale features. In the near future, we will be studying the 10-Hz data in the Gulf of Mexico to analyze the submesoscale features that occur on the periphery of the Loop Current.

As of this writing, the community is attempting to fund the follow-on altimeter mission, Jason-2, with a wide-swath altimeter payload (Fu 2003). For mesoscale studies, the Rossby radius of deformation is the important length scale and the cross-track resolution that is nearly nonexistent with a single altimeter will be well sampled by a wide-swath ocean altimeter (WSOA). Because the noise characteristics of the interferometric synthetic aperture radar are white, the optimal operator presented will be an important tool for computing the full (along and cross track) components of geostrophic velocity from this type of instrument. Optimal techniques for computing other higher-order derivatives of geophysical interest such as vorticity and Reynolds stresses can also be derived allowing for accurate study of the global ocean eddy fields as mapped by a WSOA. These techniques will be the focus of future techniques work.

Acknowledgments. We would like to thank the anonymous reviewers for their many detailed comments. Support was provided by NASA Contract 1221120.

APPENDIX A

"Truncation" Error Calculation

Consider a central finite-difference scheme used to minimize the truncation error of the first derivative. The coefficients of a central difference formula that minimize the truncation error are computed with a standard Taylor series expansion,

$$h_{i+1} \approx h_i + \sum_{j=1}^{J} \frac{1}{j!}(n\Delta t)^j \frac{\partial^j h}{\partial t^j}, \tag{A1}$$

where n is the number of points away from the current evaluation point, h_i, and J is the order of precision to carry out. As an example, the coefficients of the five-point central difference (two on either side) are computed as follows.

Consider each difference term using (A1):

$$\begin{aligned}
h_{i+2} - h_i &= 2\Delta t\frac{\partial h}{\partial t} + 2\Delta t^2\frac{\partial^2 h}{\partial t^2} + 1.333\Delta t^3\frac{\partial^2 h}{\partial t^3} + 0.667\Delta t^4\frac{\partial^4 h}{\partial t^4} + 0.267\Delta t^5\frac{\partial^5 h}{\partial t^5} + \cdots \\
h_{i+1} - h_i &= \Delta t\frac{\partial h}{\partial t} + 0.5\Delta t^2\frac{\partial^2 h}{\partial t^2} + 0.167\Delta t^3\frac{\partial^3 h}{\partial t^3} + 0.042\Delta t^4\frac{\partial^4 h}{\partial t^4} + 0.0083\Delta t^5\frac{\partial^5 h}{\partial t^5} + \cdots \\
h_i - h_{i-1} &= \Delta t\frac{\partial h}{\partial t} - 0.5\Delta t^2\frac{\partial^2 h}{\partial t^2} + 0.167\Delta t^3\frac{\partial^3 h}{\partial t^3} - 0.042\Delta t^4\frac{\partial^4 h}{\partial t^4} + 0.0083\Delta t^5\frac{\partial^5 h}{\partial t^5} + \cdots \\
h_i - h_{i-2} &= 2\Delta t\frac{\partial h}{\partial t} - 2\Delta t^2\frac{\partial^2 h}{\partial t^2} + 1.333\Delta t^3\frac{\partial^3 h}{\partial t^3} - 0.667\Delta t^4\frac{\partial^4 h}{\partial t^4} + 0.267\Delta t^5\frac{\partial^5 h}{\partial t^5} + \cdots.
\end{aligned} \tag{A2}$$

Now, to find the combination of these terms that minimize the truncation error in a central difference scheme, solve for

$$w_2(h_{i+2} - h_i + h_i - h_{i-2}) + w_1(h_{i+1} - h_i + h_i - h_{i-1}) \tag{A3}$$

and substitute from (A2):

$$w_2(h_{i+2} - h_{i-2}) + w_1(h_{i+1} - h_{i-1}) = w_2\left(4\Delta t\frac{\partial h}{\partial t} + 2.667\Delta t^3\frac{\partial^3 h}{\partial t^3} + 0.533\Delta t^5\frac{\partial^5 h}{\partial t^5}\right) + \cdots w_1\left(2\Delta t\frac{\partial h}{\partial t} + 0.333\Delta t^3\frac{\partial^3 h}{\partial t^3} + 0.0167\Delta t^5\frac{\partial^5 h}{\partial t^5}\right). \quad \text{(A4)}$$

Solving for w_1 and w_2 to eliminate the smallest order term (in this case, Δt^3), we find that $w_1 = 8$ and $w_2 = -1$, giving

$$-(h_{i+2} - h_{i-2}) + 8(h_{i+1} - h_{i-1}) = -12\Delta t\frac{\partial h}{\partial t} + 0.4\Delta t^5\frac{\partial^5 h}{\partial t^5}. \quad \text{(A5)}$$

Solving for $\partial h/\partial t$,

$$\frac{\partial h}{\partial t} = \frac{h_{i+2} - h_{i-2} - 8h_{i+1} + 8h_{i-1}}{-12\Delta t} - 0.033\Delta t^4\frac{\partial^5 h}{\partial t^5} = -0.167\left(\frac{h_{i+2} - h_{i-2}}{2\Delta t}\right) + 0.667\left(\frac{h_{i+1} - h_{i-1}}{\Delta t}\right) - 0.033\Delta t^4\frac{\partial^5 h}{\partial t^5}. \quad \text{(A6)}$$

Therefore, this system is fourth-order accurate $O(\Delta t^4)$ and the coefficients for this operator are $c_{-2} = c_2 = -0.167$ and $c_{-1} = c_1 = 0.667$. To test this result, apply these coefficients to operator (3) with ($p = -2$ and $q = 2$):

$$\Delta_{4t}^{-2,2} = -0.167\left(\frac{h_{i+2} - h_i}{2\Delta t}\right) + 0.667\left(\frac{h_{i+1} - h_i}{\Delta t}\right) + \cdots 0.667\left(\frac{h_i - h_{i-1}}{\Delta t}\right) - 0.167\left(\frac{h_i - h_{i-2}}{2\Delta t}\right). \quad \text{(A7)}$$

Combining with the results from (A2), the operation simplifies to

$$\frac{\partial h}{\partial t} = 0.0667\Delta t^4\frac{\partial^5 h}{\partial t^5} + \cdots, \quad \text{(A8)}$$

confirming the results of a fourth-order accurate calculation.

Using the method above, the accuracy of the optimal difference operator described in this paper can be calculated for any given size. As an example, we shall present the solution for the truncation error in the $T = 5$ symmetric case (i.e., an operator using two points on either side of the current). Substituting (A2) into (3) and using the symmetric coefficients from Table 1 results in

$$\Delta_{4t}^{-2,2} = \frac{\partial h}{\partial t} = -1.133\Delta t^2\frac{\partial^3 h}{\partial t^3} - 0.217\Delta t^4\frac{\partial^5 h}{\partial t^5} + \cdots, \quad \text{(A9)}$$

illustrating that the optimal five-point operator is second-order accurate in $O(\Delta t^2)$. Applying operator (3) for nonsymmetric optimal cases also results in a second-order approximation accuracy.

APPENDIX B

Optimal Weighting Coefficient Code

A function to calculate the optimal weighting coefficients as presented in this paper is included. The code listing is designed for use with Matlab by The Math Works, Inc.

```
function [cn, error] = genweights(p, q, dt)
% function [cn, error] = genweights(p, q, dt)
% Given p and q, return the vector of c_n's: the optimal weighting
% coefficients and the noise reduction factor of h.
%
% p is the number of points before the point of interest (always negative)
% q is the number of points after the point of interest (always positive)
% dt is the sampling period (defaults to 1 s)
%
% Written by Brian Powell (c) 2004, University of Colorado, Boulder

if ( nargin < 2 )
   error('Incorrect Arguments');
elseif ( nargin < 3 )
   dt = 1;
end
```

```
% Do some verification
p = max(p,−p);
q = max(q,−q);
if ( −p > q)
   error (‘p must be less than q’);
end

% Build the matrices
N = abs(p) + abs(q);
T = N + 1;
A = zeros(T,T);
A(T,:) = [ ones(1,N) 0 ];
n = [ −p:q ];
n = n(find(n~=0));
for i=1:length(n),
   A(i,:) = [ 1./n.*(−n(i)/2) n(i)^2*dt^2/4 ];
   A(i,i) = −1;
end
B = zeros(T,1);
B(end) = 1;

% Compute the coefficients
cn = A\B;
cn = cn(1:end−1);

% Compute the error
error = sqrt( sum(cn’./(n*dt))^2 + sum( (cn’./(n*dt)).^2 ) );
```

REFERENCES

Chelton, D. B., R. A. deSzoeke, M. G. Schlax, K. El Naggar, and N. Siwertz, 1998: Geographical variability of the first baroclinic Rossby radius of deformation. *J. Phys. Oceonogr.*, **28,** 433–460.

Fu, L. L., Ed., 2003: Wide-swath altimetric measurement of ocean surface topography. JPL Publication 03-002, 67 pp.

——, and A. Cazenave, 2001: *Satellite Altimetry and Earth Sciences: A Handbook of Techniques and Applications.* Academic Press, 463 pp.

——, E. J. Christensen, C. A. Yamarone Jr., M. Lefebvre, Y. Ménard, M. Dorrer, and P. Escudier, 1994: TOPEX/POSEIDON mission overview. *J. Geophys. Res.*, **99,** 24 369–24 381.

Leeuwenburgh, O., and D. Stammer, 2002: Uncertainties in altimetry-based velocity estimates. *J. Geophys. Res.*, **107,** 3175, doi:10.1029/2001JC000937.

Morrow, R., R. Coleman, J. Church, and D. Chelton, 1994: Surface eddy momentum flux and velocity variances in the Southern Ocean from Geosat altimetry. *J. Phys. Oceanogr.*, **24,** 2050–2071.

Ohlmann, J. C., P. P. Niiler, C. A. Fox, and R. R. Leben, 2001: Eddy energy and shelf interactions in the Gulf of Mexico. *J. Geophys. Res.*, **106,** 2605–2620.

Peyret, R., and T. D. Taylor, 1983: *Computational Methods for Fluid Flow.* Springer-Verlag, 358 pp.

Qiu, B., 1995: Variability and energetics of the Kuroshio Extension and its recirculation gyre from the first two-year TOPEX data. *J. Phys. Oceanogr.*, **25,** 1827–1842.

Schlax, M. G., and D. B. Chelton, 1992: Frequency domain diagnostics for linear smoothers. *J. Amer. Stat. Assoc.*, **87,** 1070–1081.

Stammer, D., 1997: Global characteristics of ocean variability estimated from regional TOPEX/Poseidon altimeter measurements. *J. Phys. Oceanogr.*, **27,** 1743–1769.

Strub, P. T., T. K. Chereskin, P. P. Niiler, C. James, and M. D. Levine, 1997: Altimeter-derived variability of surface velocities in the California Current system. *J. Geophys. Res.*, **102,** 12 727–12 748.

Taylor, J. R., 1982: *An Introduction to Error Analysis: The Study of Uncertainties in Physical Measurements.* University Science Books, 270 pp.

Yale, M. M., 1997: Modeling upper mantle rheology with numerical experiments and mapping marine gravity with satellite altimetry. Ph.D. thesis, University of California, San Diego, 118 pp.

——, D. T. Sandwell, and W. H. F. Smith, 1995: Comparison of along-track resolution of stacked Geosat, *ERS-1*, and TOPEX satellite altimeters. *J. Geophys. Res.*, **100,** 15 117–15 127.

Zlotnicki, V., 1994: Correlated environmental corrections in TOPEX/POSEIDON, with a note on ionospheric accuracy. *J. Geophys. Res.*, **99,** 24 907–24 914.